RSC Advances

PAPER

View Article Online
View Journal | View Issue

Open Access Article. Published on 19 October 2018. Downloaded on 3/13/2026 2:54:15 AM.
This article is licensed under a Creative Commons Attribution-NonCommercial 3.0 Unported Licence.

Check for updates

Cite this: *RSC Adv.*, 2018, **8**, 35735

Retention and diffusion of transmutation H and He atoms in $Be_{12}Ti$: first-principles calculations

Xiaolu Zhu,[ab] Canglong Wang,*[b] Jiajia Liu,[ab] Xingming Zhang,[c] Huiqiu Deng,[d] Wenshan Duan*[a] and Lei Yang[b]

Received 12th August 2018
Accepted 5th October 2018

DOI: 10.1039/c8ra06768f

rsc.li/rsc-advances

The beryllide $Be_{12}Ti$ is considered to be the most promising candidate material for advanced plasma facing materials in future fusion reactors because of its excellent performance. In this work, first-principles calculations were conducted to gain insight into the retention and diffusion behavior of transmutation H and He atoms in $Be_{12}Ti$. The solution energy and migration energy of single impurity H/He atoms were computed to study the behavior of their retention and diffusion. Among seven stable interstitial sites, H atoms preferentially occupy the octahedral interstitial site, I_{oct}, whereas He atoms preferentially occupy the dodecahedral interstitial site, I_{dode}. The solubility of H is much higher than that of He in $Be_{12}Ti$. When monovacancy is generated, H atoms preferentially stay in the vicinity of Be1 vacancies, while He atoms tend to reside in the center of Ti vacancies. The migration energy barrier of a single He atom between first near-neighbor I_{dode} sites is 0.35 eV. For H atoms, the migration energy barrier from I_{dode} to I_{tetra2} is 0.45 eV. The barrier along the paths I_{tri1}–I_{dode}–I_{tri1} is 0.38 eV. When a Be3 vacancy is introduced as the neighbour of I_{tri1}, the migration energy barrier increases to 0.77 eV. These results indicate that vacancies can trap impurity atoms and may act as seeds for bubble formation.

1 Introduction

For future nuclear applications – such as the DEMO reactor – plasma facing materials (PFMs) would experience high flux particles (H isotopes and He), high-energy neutron irradiation, heat flux, thermomechanical stress, surface sputtering and erosion, *etc.* The blanket material may need to withstand the severe conditions of high temperatures up to 600–900 °C, high neutron doses of ~50 dPa, and high He generation (~20 000 appm).[1] Therefore, advanced PFMs are urgently desired and beryllium intermetallic compounds (beryllides) have been proposed as candidate materials. $Be_{12}X$ (X is Ti, V, Mo, or W) was pre-selected as one of the candidate materials due to the low radioactivity and high melting point of Ti, V, Mo, and W metals. Besides, the structure of $Be_{12}X$ has good oxidation resistance and high Be content.[2–4] Of the pre-selected beryllides, the main research has been focused on $Be_{12}Ti$ due to its relatively easy fabrication.[5,6] It was indicated that the compatibility between $Be_{12}Ti$ and the structural material SS316LN was much better than that of Be and SS316LN.[7] On the other hand, the swelling of $Be_{12}Ti$ was expected to be smaller than that of Be under high temperature neutron irradiation.[8] $Be_{12}Ti$ had fewer irradiation defects than Be under He ion and electron irradiation.[9] Furthermore, it was indicated that the amount of tritium retained in $Be_{12}Ti$ was much smaller than that in Be.[10]

However, the irradiation response of $Be_{12}Ti$ has not yet been completely clarified due to the lack of an accessible fusion environment. More work must be carried out to identify the fundamental processes occurring during irradiation damage. In particular, it is vitally important to understand how the defects are generated and lead to macroscopic changes not only by means of experiments but also with numeric simulations. First-principles density functional theory (DFT) is a powerful and reliable tool for exploring the atomistic behavior of defects in materials.[11,12] So far, there has been relatively little theoretical effort devoted to the study of the performance of $Be_{12}Ti$ in nuclear reactors. Jackson *et al.* have investigated the stability of intrinsic point defects (self-interstitial atoms and vacancies) and the interactions between them in $Be_{12}X$ using DFT simulations.[13] Peng *et al.* have conducted theoretical investigations on the structural, elastic and electronic properties under pressure.[14,15]

In addition, H and He impurities are inevitably generated in the blanket materials due to transmutation reactions. The aggregation and accumulation of them will result in the formation of H/He bubbles, and finally the degradation of the mechanical properties, such as swelling, creep, and embrittlement, which have been validated in various metals.[16–19] Unfortunately, so far there have been few theoretical simulation

[a]College of Physics and Electronic Engineering, Northwest Normal University, Lanzhou 730070, China. E-mail: duanws@nwnu.edu.cn

[b]Institute of Modern Physics, Chinese Academy of Sciences, Lanzhou 730000, China. E-mail: clwang@impcas.ac.cn

[c]College of Science, Hunan Agricultural University, Changsha 410128, China

[d]Department of Applied Physics, School of Physics and Electronics, Hunan University, Changsha 410082, China

Open Access Article. Published on 19 October 2018. Downloaded on 3/13/2026 2:54:15 AM.
This article is licensed under a Creative Commons Attribution-NonCommercial 3.0 Unported Licence.

studies on the behaviour of the impurity H and He atoms in $Be_{12}Ti$. Only the solution energy of H in $Be_{12}Ti$ has been determined using first-principles electronic structure methods.[20] Atomistic simulations are helpful for a better understanding of the properties of defects due to inaccessible observation from experiments.

In order to better understand the behavior of H and He atoms in $Be_{12}Ti$, the fundamental properties of retention and diffusion processes for H and He atoms have to be studied from first principles. In the present work, the primary research concentrates on the stable positions of interstitial H and He atoms and individual H and He atoms within monovacancies, the lowest-energy diffusion path and corresponding migration energies. This paper is organized as follows: in Section 2, after a brief description of the computational methodology including parameter settings, the crystal structure of $Be_{12}Ti$ is described; the detailed simulation results and discussion are presented in Section 3; and a brief conclusion is given in Section 4.

2 Computational methodology

All first-principles calculations were performed using the Vienna Ab initio Simulation Package (VASP)[21,22] using the plane-wave pseudo-potential approach.[23,24] The projector-augmented wave (PAW) potentials[25,26] for the ion–electron interaction and the generalized gradient approximation (GGA) with a PW91 functional[27] for the exchange–correlation interaction are adopted. A tetragonal supercell of 2 × 2 × 2 containing 208 atoms was used for all defect calculations. The Brillouin zone was sampled with 2 × 2 × 4 *k*-point meshes generated with the Monkhorst–Pack scheme[28] and a cutoff energy of 500 eV was employed to describe the interactions of impurity H/He atoms in $Be_{12}Ti$. During geometry optimization, all atomic positions were fully relaxed at a constant cell volume until there were energy changes on each atom of less than 1×10^{-6} eV and forces on each atom of less than 0.001 eV $Å^{-1}$. These parameters, including *k*-point and cutoff energy convergence, have been proved to be sufficient to give a well-converged total energy. The climbing image nudged elastic band (CI-NEB) method[29,30] was used to determine the minimum energy paths and the migration barriers of impurity H/He atoms in bulk $Be_{12}Ti$.

The crystal structure of $Be_{12}Ti$ shows tetragonal symmetry with the space group I_4/mmm.[31] Ti atoms occupy the Wyckoff position of the 2a lattice site (0,0,0), Be atoms occupy three symmetrically distinct sites within the structure, here labeled Be1, Be2, and Be3, which occupy the Wyckoff positions of 8f (0.25,0.25,0.25), 8i (0.361,0,0), and 8j (0.277,0.5,0), respectively. The structure of the unit cell for tetragonal $Be_{12}Ti$ is shown in Fig. 1, where red balls, yellow balls, orange balls, and green balls denote Be1 atoms, Be2 atoms, Be3 atoms, and Ti atoms, respectively. In our calculations, the equilibrium lattice parameters of tetragonal $Be_{12}Ti$ were $a = b = 7.33$ Å and $c = 4.14$ Å, which are in good agreement with the experimental values ($a = b = 7.35$ Å and $c = 4.19$ Å)[32] and the CASTEP calculation results ($a = b = 7.361$ Å and $c = 4.163$ Å).[13] This ensures the accuracy of the present first-principles calculations.

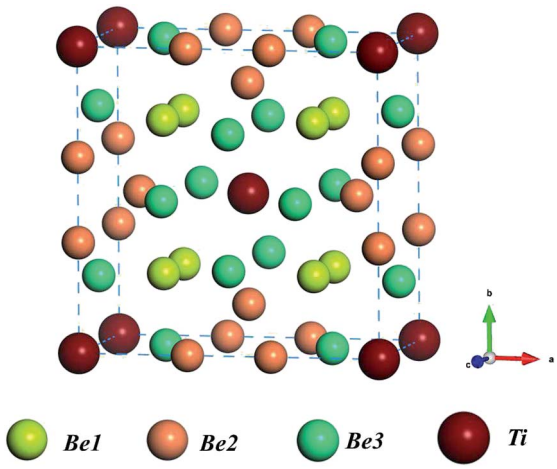

Fig. 1 Schematic of the unit cell of the $Be_{12}Ti$ crystal structure; red balls, yellow balls, orange balls, and green balls denote Be1 atoms, Be2 atoms, Be3 atoms, and Ti atoms, respectively.

3 Results and discussion

3.1 Individual H and He in bulk $Be_{12}Ti$

To investigate the solution state of H/He impurity atoms in the $Be_{12}Ti$ lattice, we chose 20 sets of interstitial sites in the unit cell of $Be_{12}Ti$ as the initial locations of H/He atoms. After relaxation, seven stable interstitial sites were found, as shown in Fig. 2: an octahedral interstitial site (I_{oct}) surrounded by four Be3 atoms and two Ti atoms, a tetrahedral interstitial site (I_{tetra1}) surrounded by four Be2 atoms, a trigonal-bipyramid interstitial site (I_{tri1}) surrounded by five atoms (two Be1 atoms, two Be2 atoms, and one Ti atom), a tetrahedral interstitial site (I_{tetra2}) surrounded by four atoms (Ti atom, Be1 atom, and two Be3 atoms), a trigonal-bipyramid interstitial site (I_{tri2}) surrounded by four Be2 atoms and one Be3 atom, a dodecahedral interstitial site (I_{dode}) surrounded by six Be2 atoms and two Be3 atoms, and another tetrahedral interstitial site (I_{tetra3}) surrounded by four atoms (two Be1 atoms, one Be2 atom, and one Be3 atom). To determine the most preferential site for impurity H/He atoms, the solution energies of H/He atoms in these interstitial sites were calculated by:[33]

$$E^{s}_{H}(\text{int}) = E(n\text{A} + \text{H}) - E(n\text{A}) - E(\text{H}_2)/2 \quad (1)$$

and

$$E^{s}_{He}(\text{int}) = E(n\text{A} + \text{He}) - E(n\text{A}) - E(\text{He}) \quad (2)$$

respectively, where A denotes the host lattice of $Be_{12}Ti$, n is the number of atoms in a supercell without defects; $E(n\text{A})$ is the energy of a perfect supercell; $E(n\text{A} + \text{H/He})$ is the energy of a supercell with an interstitial H/He atom; $E(\text{H}_2)/2$ is one half of the energy of a gas-phase H_2 molecule, which is −3.385 eV according to our calculation; $E(\text{He})$ is the energy of an isolated He atom. By definition, a positive solution energy denotes endothermicity, while a negative solution energy denotes exothermicity. The zero-point energy (ZPE) should be taken into

 This journal is © The Royal Society of Chemistry 2018

Open Access Article. Published on 19 October 2018. Downloaded on 3/13/2026 2:54:15 AM.
This article is licensed under a Creative Commons Attribution-NonCommercial 3.0 Unported Licence.

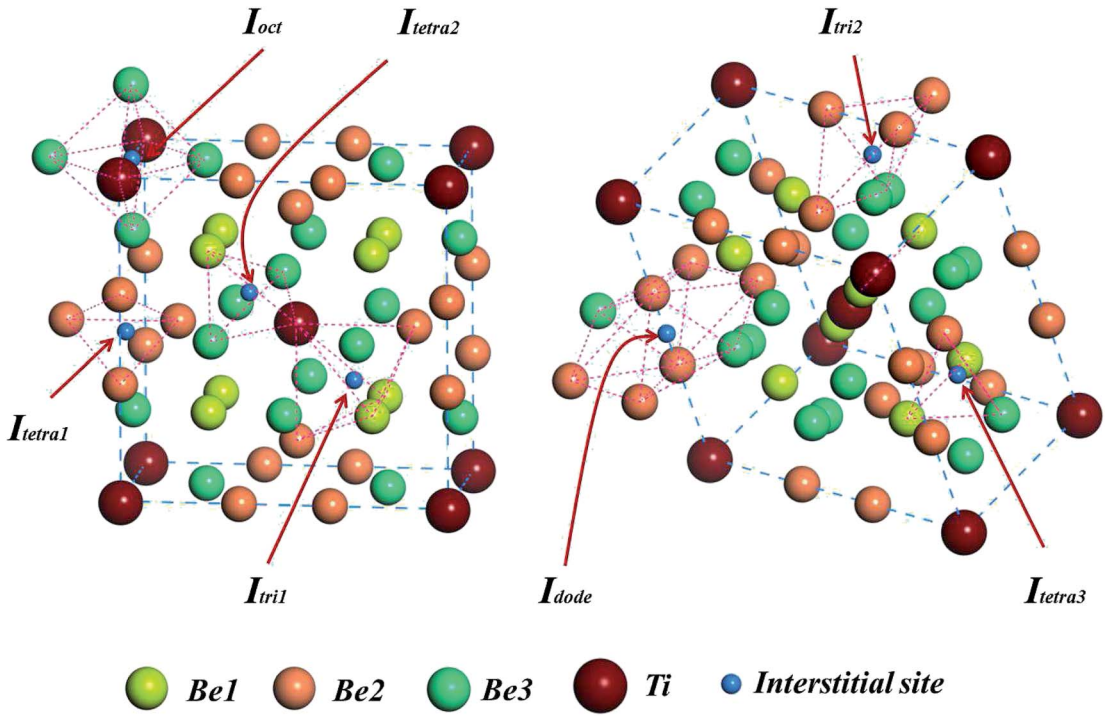

Fig. 2 Seven energetically favorable interstitial configurations within a unit cell of the $Be_{12}Ti$ structure.

consideration in the system involving light elements, which is calculated by $\mathrm{ZPE} = \sum_i h\nu_i/2$, where h is the Planck constant and ν is the real normal mode frequency. The ZPE-corrected H solution energy should be defined as:[34]

$$E_{\mathrm{H}}^{\mathrm{s}}(\mathrm{int})_{\mathrm{ZPE}} = E_{\mathrm{H}}^{\mathrm{s}}(\mathrm{int}) + \Delta\mathrm{ZPE} = E_{\mathrm{H}}^{\mathrm{s}}(\mathrm{int}) + \{\mathrm{ZPE}(n\mathrm{A} + \mathrm{H}) - \mathrm{ZPE}(n\mathrm{A}) - \mathrm{ZPE}(\mathrm{H}_2)/2\} \quad (3)$$

Since the vibrations of the bulk metal are negligible compared to those of atomic H in an interstitial site, ZPE(nA) was ignored and ZPE(nA + H) was replaced with ZPE(H) in our calculations. ZPE(H_2) is 0.28 eV. The ZPE-corrected He solution energy is similar to eqn (3). ZPE(He) is about 0.01 eV. The solution energies of interstitial H/He atoms and the corresponding ZPE-corrected solution energies are all shown in Table 1. As we can see, the solution energies of interstitial H/He atoms are positive, which means that the incorporation of impurity H/He atoms is always an endothermic process. Since He atoms have a closed-shell electronic structure and bonding interactions are small, its solubility in materials is extremely low.[35,36] The solubility of H atoms in materials can vary as the phase structure changes. For example, the solutions of H atoms in Fe, Ni, W, Be, Pt, Cu, Ag and Au are endothermic, while those in V, Ti, Nb, Ta and Pd are exothermic.[34] The solution energies of He atoms are 4.03 eV, 4.38 eV, 4.53 eV, and 4.87 eV for I_{dode}, I_{tetra1}, I_{oct} and I_{tri1}, respectively. After relaxation, He atoms at I_{tetra2}, I_{tetra3}, and I_{tri2} interstitial sites have been proved to be unstable: the interstitial He atom at I_{tetra2} or I_{tetra3} will diffuse to I_{dode} and the He atom at I_{tri2} will diffuse to I_{oct}. It is indicated that I_{dode} is the most energetically favorable site for a single He atom in $Be_{12}Ti$. The dodecahedron has a larger volume than other polyhedra, which provides a lower charge density for the accommodation of He atoms. For interstitial H atoms, the sequence of solution energies is $I_{\mathrm{oct}} < I_{\mathrm{tetra2}} < I_{\mathrm{tri2}} < I_{\mathrm{tetra1}} < I_{\mathrm{tri1}} < I_{\mathrm{tetra3}} < I_{\mathrm{dode}}$. The solution energy is lowest at I_{oct}, with 0.50 eV. However, the solution energy is largest at I_{dode}, with 1.30 eV. It is indicated that H atoms preferentially occupy I_{oct}. I_{tetra1}, I_{tri1} and I_{tri2} have nearly equal solution energies. I_{oct} sites are surrounded by four Be3 atoms and two Ti atoms. I_{dode} sites are surrounded by six Be2 atoms and two Be3 atoms. The solution of H atoms into Be metal is endothermic, while the solution of H atoms in Ti metal is exothermic, that is the interactions of H atoms with Ti atoms are stronger those that of H atoms with Be atoms, so H atoms preferentially occupy the I_{oct} site. As a distinct difference between the interstitial H and He, the solution energy of H is substantially lower than that of He, indicating that the solubility of H in $Be_{12}Ti$ is much higher than that of He, which is similar to that of Be metal.[37] In addition, the effect of ZPE on the solution energies of interstitial H/He varies from 0.03 to 0.11 eV, and the preferential site for H/He atoms in bulk $Be_{12}Ti$ remains unchanged after ZPE correction.

Table 1 Solution energies of single H and He atoms in $Be_{12}Ti$

Configuration	I_{oct}	I_{dode}	I_{tetra1}	I_{tetra2}	I_{tetra3}	I_{tri1}	I_{tri2}
$E_{\mathrm{H}}^{\mathrm{s}}(\mathrm{int})$	0.50	1.30	0.94	0.80	1.20	0.98	0.92
$E_{\mathrm{H}}^{\mathrm{s}}(\mathrm{int})_{\mathrm{ZPE}}$	0.57	1.40	1.06	0.93	1.36	1.07	1.05
$E_{\mathrm{He}}^{\mathrm{s}}(\mathrm{int})$	4.53	4.03	4.38	—	—	4.87	—
$E_{\mathrm{He}}^{\mathrm{s}}(\mathrm{int})_{\mathrm{ZPE}}$	4.58	4.10	4.42	—	—	4.98	—

Open Access Article. Published on 19 October 2018. Downloaded on 3/13/2026 2:54:15 AM.
This article is licensed under a Creative Commons Attribution-NonCommercial 3.0 Unported Licence.

To interpret the difference of H/He occupation in perfect $Be_{12}Ti$, Fig. 3 shows the site-projected electronic density of states (DOS) of H/He interstitial defects and the nearest-neighbor metal atom in $Be_{12}Ti$. As we can see from Fig. 3(a) and (b), the embedded H/He atoms cause distortion of the DOS of the neighboring Ti and Be metal atoms, which indicates ongoing hybridization. Larger distortion of the DOS at the metal site corresponds to the larger solution energy of H/He defects. Fig. 3(c) shows the s-projected DOS of H at I_{oct}, I_{dode}, I_{tetra1}, and I_{tetra2}. Fig. 3(d) shows the p-projected DOS of He at I_{oct}, I_{dode}, I_{tetra1}, and I_{tri1}. The position of the Fermi energy level relative to the peaks in the DOS determines the occupation of the states and the nature of the bonding.[38] The lower the DOS at the Fermi energy level, the more energetically favorable the corresponding defect configuration. It can be seen from Fig. 3(c) that the interaction of I_{oct} H with its neighbor metal atoms leads to a lower DOS at the Fermi energy level than that of other H interstitials, which indicates the stronger bonding at the I_{oct} site. The DOSs of He interstitials at the Fermi energy level rank in a sequence of $I_{dode} < I_{tetra1} < I_{oct} < I_{tri1}$, which is in agreement with the order of the site preference of He in $Be_{12}Ti$.

3.2 Individual H/He within a monovacancy in $Be_{12}Ti$

As a PFM for nuclear energy applications, $Be_{12}Ti$ is inevitably subject to high temperatures and particle fluxes that induce the generation of large numbers of vacancies. Four types of vacancy can be formed in bulk $Be_{12}Ti$ under irradiation. The formation energies of the vacancies were calculated using the following formula:

$$E^{f}_{VA} = E((n-1)A) - E(nA) + E(Be/Ti) \quad (4)$$

where $E((n-1)A)$ is the energy of a supercell with a vacancy and $E(Be/Ti)$ is the chemical potential of the Be or Ti host. Hexagonal close-packed bulk Be and Ti are adopted as the reference elemental Be and Ti solids, respectively. The formation energies of the vacancies are listed in Table 2. It can be seen that the Be2 vacancy has the lowest formation energy of 1.44 eV, which indicates that the Be2 vacancy is easier to form than the other types of vacancy in $Be_{12}Ti$. The formation energy of the Ti vacancy of 3.92 eV is much larger than that of the Be vacancies, indicating that the formation of Ti vacancies is very difficult in $Be_{12}Ti$. The present results are in good agreement with the previous CASTEP results.[13]

The theoretical and experimental research demonstrates that vacancies can reduce the charge density of their vicinity, leading to the aggregation and binding of impurity atoms at

Table 2 Vacancy (VA) formation energies (E^{f}_{VA}) in $Be_{12}Ti$

Configuration	VA_{Be1}	VA_{Be2}	VA_{Be3}	VA_{Ti}
This work	1.65	1.44	1.56	3.92
Previous work[13]	1.60	1.43	1.53	4.10

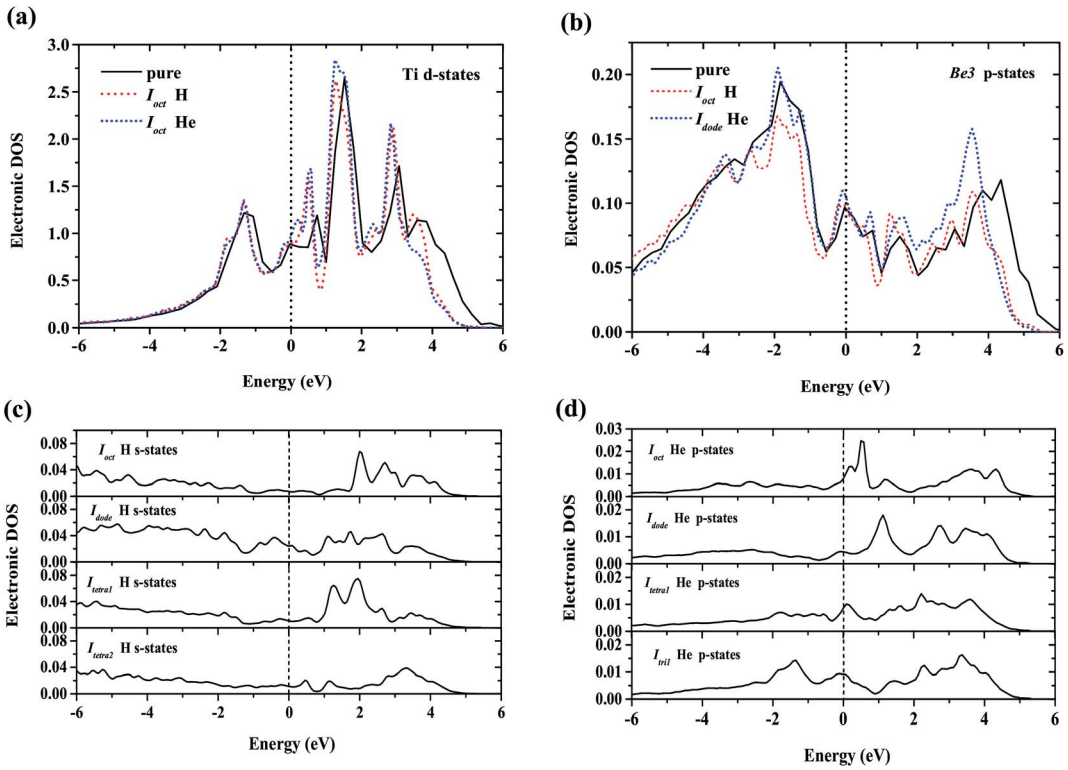

Fig. 3 (a) Local DOS for H/He nearest-neighbor Ti atom; (b) local DOS for H/He nearest-neighbor Be3 atom; (c) local DOS for interstitial H atoms – the s-projected DOS of H at I_{oct}, I_{dode}, I_{tetra1}, and I_{tetra2}; (d) local DOS for interstitial He atoms – the p-projected DOS of He at I_{oct}, I_{dode}, I_{tetra1}, and I_{tri1}. The Fermi energy of the supercell with the H/He defect is 0.00 eV.

Open Access Article. Published on 19 October 2018. Downloaded on 3/13/2026 2:54:15 AM.
This article is licensed under a Creative Commons Attribution-NonCommercial 3.0 Unported Licence.

these sites.[39,40] Thus, it is important to shed light on the capacity of the four types of vacancy to trap H/He atoms. The solution energies for single H/He atoms within monovacancies in $Be_{12}Ti$ are computed as follows:

$$E^{s}_{H}(VA) = E((n-1)A + H) - E((n-1)A) - E(H_2)/2 \quad (5)$$

and

$$E^{s}_{He}(VA) = E((n-1)A + He) - E((n-1)A) - E(He) \quad (6)$$

respectively. What is the most preferential position for a single H/He atom in a $Be_{12}Ti$ solid containing a monovacancy? Several possible initial positions were considered: vacancy centers and the adjacent interstitial sites of vacancies. These configurations and the corresponding solution energies of H/He are illustrated in Fig. 4 and 6, respectively, where (a)–(d) show that the H/He atoms are initially placed at a vacancy center, and (e)–(h) show that H/He atoms are initially placed at stable or metastable interstitial sites near the vacancies. The hollow circles of different colours represent corresponding vacancies; pink balls denote H atoms and dark blue balls denote He atoms. The plane direction of each schematic is labeled. In Fig. 4(a), the solution energy of H atoms at Ti vacancy centers is 2.03 eV, which is less favorable than that of interstitial H sites in perfect $Be_{12}Ti$. When placing H at an I_{oct} site near a Ti vacancy, its solution energy reduces to 0.17 eV as shown in Fig. 4(e). After relaxation, a H atom at I_{tetra2} close to a Be1 vacancy moves 0.35 Å towards the Be1 vacancy with $E^s = -0.26$ eV, which is much lower than that of H staying at the Be1 vacancy center ($E^s = 0.78$ eV) as shown in Fig. 4(b) and (f). A H atom within a Be2 vacancy center moves towards a Ti atom by a distance of 0.765 Å with a solution energy of 0.06 eV, as shown in Fig. 4(c). When putting H at an I_{tetra2} site near a Be2 vacancy, it shifts towards the Be2 vacancy by 1.24 Å with $E^s = -0.17$ eV, as shown in Fig. 4(g). A H atom at a Be3 vacancy center moves to I_{oct} with $E^s = -0.01$ eV, as shown in Fig. 4(d). In conclusion, H atoms preferentially occupy the neighbouring interstitial sites of the vacancy rather than the vacancy center. The capacity for vacancy trapping single H atoms follows the order $VA_{Be1} > VA_{Be2} > VA_{Be3} > VA_{Ti}$.

To describe the behaviour of H preferentially occupying the neighbouring interstitial sites of a vacancy rather than the vacancy center, we have computed the local densities of states (LDOS) of selected H and their nearest-neighbor metal atoms. As shown in Fig. 5(a), the p-projected DOSs of Be3 for the H in the center of VA_{Ti} and I_{oct} H within VA_{Ti} produce distortion compared to that of the pure material with a VA_{Ti}, and the DOS of Be3 for the H in the center of VA_{Ti} deforms more than that of I_{oct} H within VA_{Ti}. The s-projected DOS of H at the Fermi energy level for H in the center of VA_{Ti} is larger than that of I_{oct} H within VA_{Ti}, as shown in Fig. 5(b). It is indicated that H in the VA_{Ti} center is less energetically stable than I_{oct} H within VA_{Ti}. The deformation of the d-projected DOSs of Ti for the H in the center of VA_{Be1} and I_{tetra2} H within VA_{Be1} compared with that of the pure material with a VA_{Be1}, as shown in Fig. 5(a), is visible, and the s-projected DOS of H at the Fermi energy level for H in the center of VA_{Be1} is slightly larger than that of I_{tetra2} H within VA_{Be1}, as shown in Fig. 5(b).

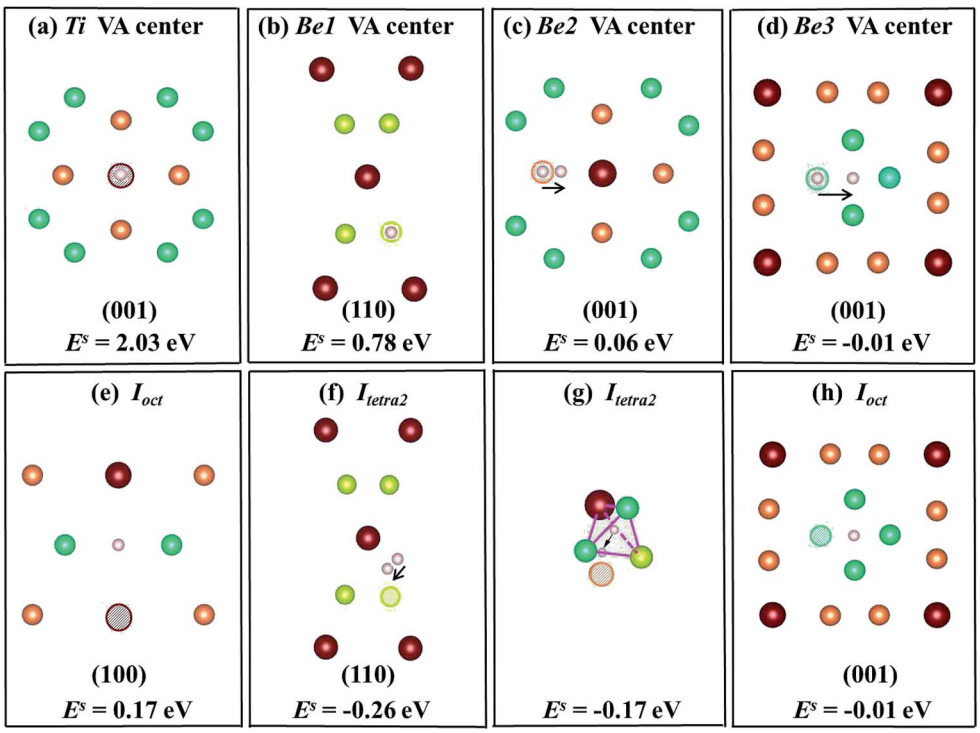

Fig. 4 Schematic diagrams and corresponding solution energies of a single H atom in the vacancy centers ((a)–(d)) and interstitial sites near vacancies ((e)–(h)) in the $Be_{12}Ti$ solid. The hollow circles of different colours represent the corresponding vacancies and pink balls denote H atoms.

Open Access Article. Published on 19 October 2018. Downloaded on 3/13/2026 2:54:15 AM.
This article is licensed under a Creative Commons Attribution-NonCommercial 3.0 Unported Licence.

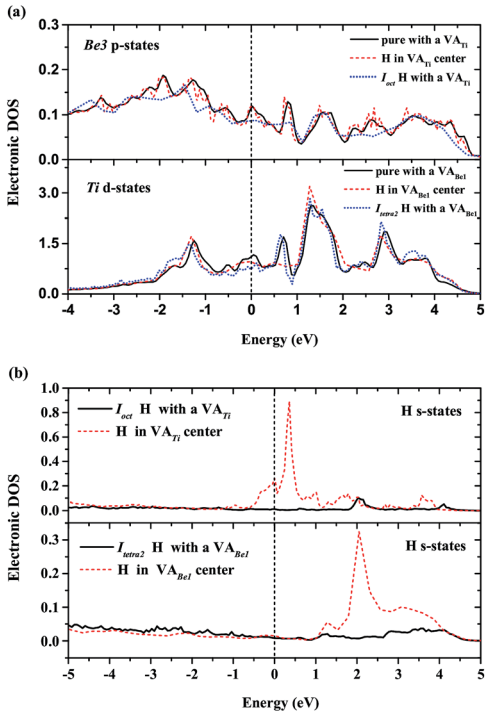

Fig. 5 (a) Local DOS for vacancy nearest-neighbor Ti and Be3 atoms; (b) local DOS for interstitial H atoms within VA_{Ti} and VA_{Be1}. The Fermi energy of the supercell with the H defect is 0.00 eV.

The most energetically preferable site for one He atom is the Ti vacancy center with the lowest solution energy of 0.94 eV (Fig. 6(a)). After relaxation, He atoms at nearest neighbouring interstitial sites, I_{oct}, spontaneously move into the Ti vacancy centers with an athermal process as shown in Fig. 6(e). The solution energy is 3.10 eV when the He atom is placed at the Be1 vacancy center (Fig. 6(b)), but the He atom at the I_{tri1} site shifts 0.74 Å towards the Be1 vacancy with a solution energy of 2.81 eV (Fig. 6(f)), which is smaller than that at the Be1 vacancy center. The He atom at the Be2 vacancy center moves to an interstitial site, which is very close to I_{dode} with a distance of only 0.37 Å. The He atom at the I_{dode} site moves nearly the same distance of 0.36 Å towards the Be2 vacancy. The solution energies in these two cases are 1.90 eV, as shown in Fig. 6(c) and (g), respectively. When a He atom is initially placed at the Be3 vacancy center, it moves 0.667 Å towards an adjacent I_{dode} site (Fig. 6(d)). As shown in Fig. 6(h), a He atom is initially located at an I_{dode} site close to the Be3 vacancy and it moves towards the Be3 vacancy and finally arrives at a position, which is 0.687 Å from the Be3 vacancy center. The two cases have the same solution energy of 2.73 eV. It follows that the capacity of vacancies for trapping single He atoms satisfies the sequence $VA_{Ti} > VA_{Be2} > VA_{Be3} > VA_{Be1}$. It was found that He atoms preferentially occupy Ti vacancy centers, which is different to H. Such trends are similar to the behaviour of H and He inside a *hcp* Be solid.[37] The solution energies of H/He within a monovacancy in the stable states are much lower than those in a perfect supercell, indicating that the impurity atoms are preferentially trapped by

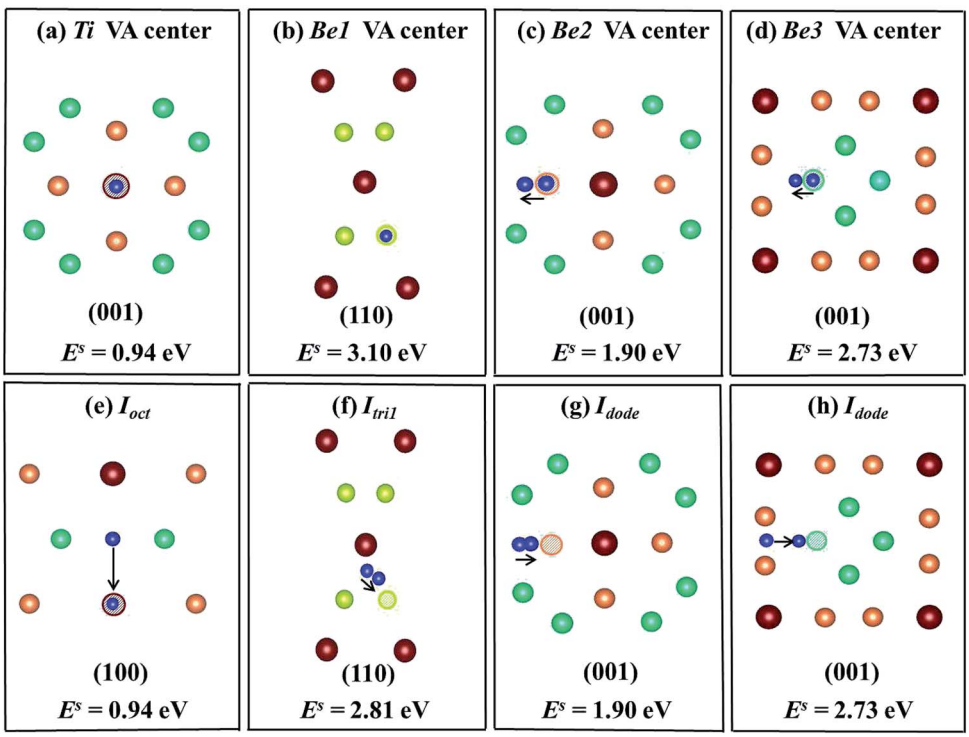

Fig. 6 Schematic diagrams and corresponding solution energies of a single He atom in the vacancy centers ((a)–(d)) and interstitial sites near vacancies ((e)–(h)) in the $Be_{12}Ti$ solid. The hollow circles of different colours represent corresponding vacancies and dark blue balls denote He atoms.

Open Access Article. Published on 19 October 2018. Downloaded on 3/13/2026 2:54:15 AM.
This article is licensed under a Creative Commons Attribution-NonCommercial 3.0 Unported Licence.

vacancies. This is accordance with the fact that a larger volume of vacancy is available for the accommodation of impurity atoms.

3.3 The diffusion of a single H/He atom in $Be_{12}Ti$

Concerning the kinetics of H/He atoms in the $Be_{12}Ti$ solid, we mainly examined the diffusion of interstitial H/He atoms, which is relevant to the initial stage after implantation or production of impurity H/He atoms. The diffusion mechanism of impurity H/He atoms was studied in terms of possible diffusion paths and the corresponding migration energies using the CI-NEB method. Here, we studied the diffusion of a single H/He atom between the relatively stable interstitial sites in a perfect $Be_{12}Ti$ solid and the diffusion of a single H/He atom from a mono-vacancy to a stable interstitial site. I_{dode} is the most energetically favorable interstitial site of He. Fig. 7 shows a path from one I_{dode} site to its first nearest-neighbor (1nn) I_{dode} site passing through an I_{tetra1} site in perfect $Be_{12}Ti$ (I_{dode}–I_{tetra1}–I_{dode}). The migration energy barrier is 0.35 eV, which is nearly equal to the migration energy of a single He along the BT–CN–BT path in Be metal.[41]

For a single H atom, I_{oct} is the most energetically favorable interstitial site. Fig. 8(a) shows a diffusion path from I_{oct} to its nearest-neighbor, I_{tetra2}. The migration energy barrier is 0.45 eV. It can be seen from Fig. 8(b) that I_{oct} is more stable than I_{tetra2} by 0.30 eV, which is in agreement with their solution energies. In Fig. 9, another diffusion path between metastable interstitial sites (I_{tri1}–I_{dode}–I_{tri1}) is also considered, where I_{dode} is the transition state. The migration energy barrier is 0.38 eV and the saddle point of the path is exactly right at the I_{dode} site. When a Be3 vacancy is introduced as the neighbour of I_{tri1}, the H atom shifts 0.23 Å towards the Be3 vacancy. The diffusion path and corresponding migration energy profile are also depicted in Fig. 9 for comparison. The migration energy increases to 0.77 eV, but the barrier of the H atom from the I_{dode} site to the Be3 vacancy is 0.20 eV. As we can see, the migration energy barrier increases when the H atom migrates from the vacancy to the interstitial site, which is attributed to the vacancy trapping of H atoms. These results imply that the diffusion of impurity atoms is relatively fast in the perfect $Be_{12}Ti$ solid. When vacancy defects exist, the diffusion of impurity atoms is impeded so that

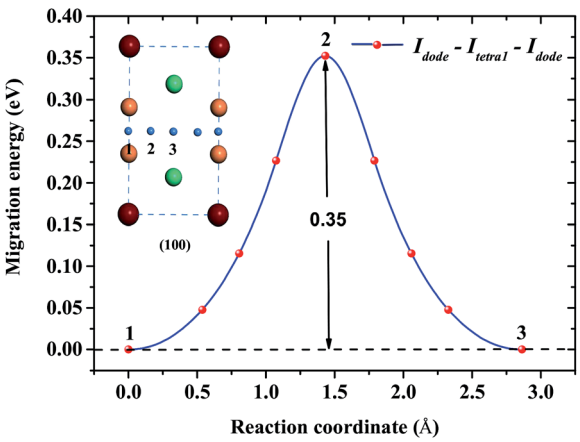

Fig. 7 Diffusion path between two 1nn I_{dode} sites passing through an I_{tetra1} site for He atoms and its migration energy profile.

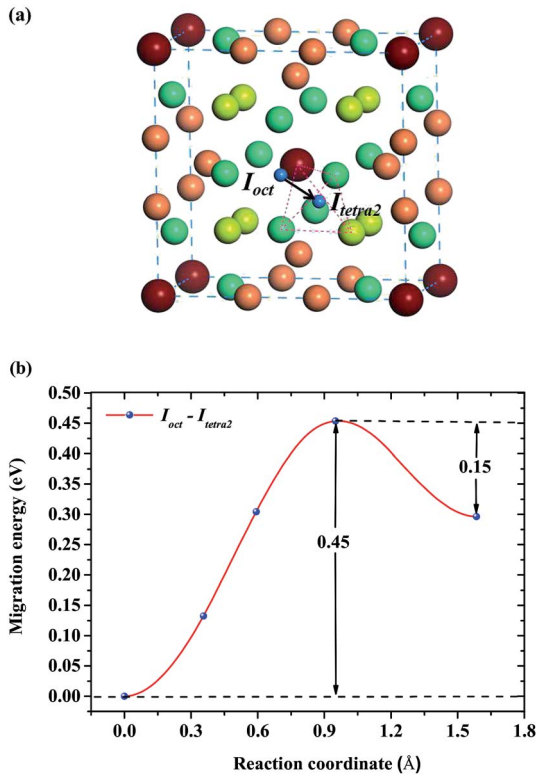

Fig. 8 (a) Diffusion path from I_{oct} to its nearest-neighbor I_{tetra2} for H atoms. (b) Corresponding migration energy profile.

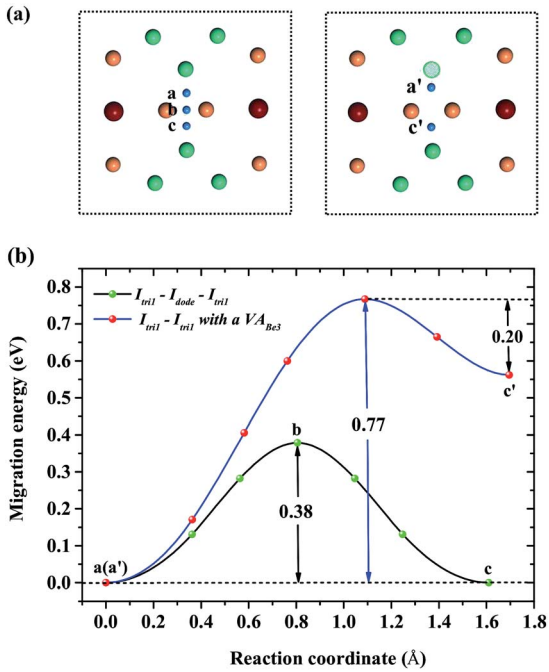

Fig. 9 (a) Diffusion paths I_{tri1}–I_{dode}–I_{tetra1} and I_{tri1}–I_{tetra1} with a VA_{Be3} for H atoms. (b) Corresponding migration energy profiles.

Open Access Article. Published on 19 October 2018. Downloaded on 3/13/2026 2:54:15 AM.
This article is licensed under a Creative Commons Attribution-NonCommercial 3.0 Unported Licence.

they cannot easily migrate, but to some extent segregate to form bubbles.

4 Summary and conclusions

The retention and diffusion behavior of H/He impurities in $Be_{12}Ti$ solid has been investigated using first-principles calculations. Among seven stable interstitial sites, H atoms preferentially occupy the octahedral interstitial site, I_{oct}, with a solution energy of 0.5 eV, whereas He atoms preferentially occupy the dodecahedral interstitial site, I_{dode}, with a solution energy of 4.03 eV. The effect of ZPE on the solution energies of H/He varies from 0.03 to 0.11 eV, and the preferential sites for H/He atoms remain unchanged after ZPE correction. The solution energy of H atoms is much lower than that of He atoms, indicating that the solubility of H atoms in $Be_{12}Ti$ is much higher than that of He atoms. When monovacancies are present in $Be_{12}Ti$, H atoms tend to stay in the vicinity of the Be1 vacancy with a solution energy of −0.26 eV, while He atoms will reside in the Ti vacancy center with a solution energy of 0.94 eV. The capacities of four types of vacancy to trap impurity atoms are different: it follows the sequence $VA_{Be1} > VA_{Be2} > VA_{Be3} > VA_{Ti}$ for single H atoms, and $VA_{Ti} > VA_{Be2} > VA_{Be3} > VA_{Be1}$ for single He atoms. The solution energies of H/He within a monovacancy in the stable states are much lower than that in a perfect supercell, indicating that the impurity atoms are preferentially trapped by vacancies. The migration energy barrier of a single He atom between first near-neighbor I_{dode} sites passing through I_{dode} is 0.35 eV. For a single H atom, the migration energy barriers from I_{oct} to its nearest-neighbor I_{tetra2} is 0.45 eV. It can be seen that the diffusion of single H/He in perfect $Be_{12}Ti$ is relatively fast due to the lower migration energy barriers. The migration energy barrier along the diffusion path I_{tri1}–I_{dode}–I_{tetra1} for a single H atom is 0.38 eV. When a Be3 vacancy is introduced as the neighbour of I_{tri1}, the barrier increases to 0.77 eV. These results imply that vacancies can trap impurity atoms and may act as seeds for bubble formation. The current first-principles results can provide the fundamental parameters for and microscopic effects of impurity H and He atoms on $Be_{12}Ti$, and are helpful to better understand the aggregation of impurity atoms and bubble formation in the early stages of irradiation damage.

Conflicts of interest

There are no conflicts to declare.

Acknowledgements

This work was supported by the National Key Research and Development Program of China (Grant No. 2016YFB0200504), the Bureau of International Cooperation, Chinese Academy of Foreign Cooperation Key Projects (Grant No. 113462KYSB20160040), the Strategic Priority Research Program of Chinese Academy of Sciences (Grant No. XDA21010202) and the National Natural Science Foundation of China (Grant No. 11747306).

References

1 K. Tsuchiya, T. Hoshino, H. Kawamura, Y. Mishima, N. Yoshida, T. Terai, S. Tanaka, K. Munakata, S. Kato, M. Uchida, M. Nakamichi, H. Yamada, D. Yamaki and K. Hayashi, *Nucl. Fusion*, 2007, **47**, 1300–1306.
2 H. Yamada, Y. Nagao, H. Kawamura, M. Nakao, M. Uchida and H. Ito, *Fusion Eng. Des.*, 2003, **69**, 269–273.
3 H. Kawamura, H. Takahashi, N. Yoshida, V. Shestakov, Y. Ito, M. Uchida, H. Yamada, M. Nakamichi and E. Ishitsuka, *Fusion Eng. Des.*, 2002, **61–62**, 391–397.
4 P. Kurinskiy, A. Moeslang, V. Chakin, M. Klimenkov, R. Rolli, S. van Til and A. A. Goraieb, *Fusion Eng. Des.*, 2013, **88**, 2198–2201.
5 M. Nakamichi and K. Yonehara, *J. Nucl. Mater.*, 2011, **417**, 765–768.
6 M. Nakamichi and J.-H. KimFusion, *Fusion Eng. Des.*, 2014, **89**, 1304–1308.
7 H. Kawamura, M. Uchida and V. Shestakov, *J. Nucl. Mater.*, 2002, **307–311**, 638–642.
8 M. Uchida, E. Ishitsuka and H. Kawamura, *J. Nucl. Mater.*, 2002, **307–311**, 653–656.
9 H. Takahashi, T. Shibayama, M. Uchida, H. Kawamura and Y. Ito, *JAERI-Rev.*, 2002, **2002-011**, 142–152.
10 N. Yoshida, H. Iwakiri, H. Kawamura and Y. Ito, *JAERI-Rev.*, 2002, **2002-011**, 58–69.
11 T. W. He, Y. H. Jiang, R. Zhou and J. Feng, *RSC Adv.*, 2016, **6**, 45250–45258.
12 J. Z. Duan, J. R. Zhang, C. L. Wang, Y. Qiu, W. S. Duan and L. Yang, *RSC Adv.*, 2014, **79**, 42014–42021.
13 M. L. Jackson, P. A. Burr and R. W. Grimes, *Nucl. Fusion*, 2017, **57**, 086049.
14 X. K. Liu, W. Zhou, X. Liu and S. M. Peng, *RSC Adv.*, 2015, **5**, 59648.
15 S. M. Peng, *J. Nucl. Mater.*, 2015, **464**, 230–235.
16 S. T. Yang, N. W. Hu, X. Q. Gou, C. L. Wang, X. L. Zhu, W. S. Duan and L. Yang, *RSC Adv.*, 2016, **6**, 59875.
17 F. Scaffidi-Argentina, G. Piazza and R. Rolli, *Fusion Eng. Des.*, 2003, **69**, 505.
18 V. P. Chakin, A. O. Posevin and I. B. Kupriyanov, *J. Nucl. Mater.*, 2007, **367–370**, 1377–1381.
19 S. P. Vagin, P. V. Chakrov, B. D. Utkelbayev, L. A. Jacobson, R. D. Field and H. Kung, *J. Nucl. Mater.*, 1998, **258–263**, 719–723.
20 Y. Fujii, M. Miyamoto, J.-H. Kim, M. Nakamichi, N. Murayoshi and H. Iwakiri, *Nuclear Materials and Energy*, 2016, **9**, 233–236.
21 G. Kresse and J. Furthmüller, *Phys. Rev. B*, 1996, **54**, 11169.
22 G. Kresse and J. Hafner, *Phys. Rev. B*, 1993, **47**, 558.
23 P. Hohenberg and W. Kohn, *Phys. Rev.*, 1964, **136**, B864.
24 W. Kohna and L. J. Sham, *Phys. Rev.*, 1965, **140**, A1133.
25 P. E. Bląğochl, *Phys. Rev. B: Condens. Matter Mater. Phys.*, 1994, **50**, 17953.
26 G. Kresse and D. Joubert, *Phys. Rev. B: Condens. Matter Mater. Phys.*, 1999, **59**, 1758.
27 J. P. Perdew and Y. Wang, *Phys. Rev. B: Condens. Matter Mater. Phys.*, 1992, **45**, 13244.

 This journal is © The Royal Society of Chemistry 2018

Open Access Article. Published on 19 October 2018. Downloaded on 3/13/2026 2:54:15 AM.
This article is licensed under a Creative Commons Attribution-NonCommercial 3.0 Unported Licence.

28 H. J. Monkhorst and J. D. Pack, *Phys. Rev. B: Condens. Matter Mater. Phys.*, 1976, **13**, 5188.
29 G. Henkelman and H. Jonsson, *J. Phys. Chem.*, 2000, **113**, 9978.
30 G. Henkelman, B. P. Uberuaga and H. Jonsson, *J. Phys. Chem.*, 2000, **113**, 9901.
31 E. Gillam, H. P. Rooksby and L. D. Brownlee, *Acta Crystallogr.*, 1964, **17**, 762–763.
32 A. Zalkin, D. E. Sands, R. G. Bedford and O. H. Krikorian, *Acta Crystallogr.*, 1961, **14**, 63–65.
33 C. Freysoldt, B. Grabowski, T. Hickel and J. Neugebauer, *Rev. Mod. Phys.*, 2014, **86**, 253–305.
34 K. Lee, M. Yuan and J. Wilcox, *J. Phys. Chem. C*, 2015, **119**, 19642–19653.
35 T. Seletskai, Y. Osetsky, R. E. Stoller and G. M. Stocks, *Phys. Rev. B: Condens. Matter Mater. Phys.*, 2015, **78**, 134103.
36 X. T. Zu, L. Yang, F. Gao, S. M. Peng, H. L. Heinisch, X. G. Long and R. J. Kurtz, *Phys. Rev. B: Condens. Matter Mater. Phys.*, 2009, **80**, 054104.
37 P. B. Zhang, J. J. Zhao and B. Wen, *J. Phys.: Condens. Matter*, 2012, **24**, 095004.
38 R. Pentcheva and M. Scheffler, *Phys. Rev. B: Condens. Matter Mater. Phys.*, 2002, **65**, 155418.
39 J. K. Nø rskov, F. Besenbacher, J. Bøttiger, B. B. Nielsen and A. A. Pisarev, *Phys. Rev. Lett.*, 1982, **49**, 1420.
40 F. Besenbacher, J. K. Nørskov, M. J. Puska and S. Holloway, *Phys. Rev. Lett.*, 1985, **55**, 852.
41 P. B. Zhang, J. J. Zhao and B. Wen, *J. Nucl. Mater.*, 2012, **423**, 164–169.